Structural and Multidisciplinary Optimization (2022) 65:112
https://doi.org/10.1007/s00158-022-03199-9

RESEARCH PAPER

# Minimum compliance with obstacle constraints: an active set approach

**Nha Van Tran**[1] · **Blaise Bourdin**[2]

Received: 23 November 2021 / Revised: 4 February 2022 / Accepted: 11 February 2022 / Published online: 10 March 2022


**Abstract**
We present a new approach to optimal design with state constraints based on active set optimization theory and implement it using a phase-field model. Our primary focus is on compliance minimization subject to inner and outer obstacles. We compare our approach to a classical penalization method and study the influence of initial guess, penalization parameters, and discretization.

**Keywords** Topology optimization · Phase-field method · Active set method · Penalization method · State constraints · Obstacle

## 1 Introduction

Topology optimization (see Bendsøe and Sigmund (2003), for a general survey) is traditionally concerned with finding the distribution of one or several materials and void optimizing some cost function subject to some constraint on admissible designs.

The typical problem structure consists of finding a partition $\mathbf{D} := (D_1, D_2, \dots, D_n)$, often referred to as the *design variable*, of a ground domain $\Omega$ minimizing an objective function $\mathcal{J}$ depending on $\mathbf{D}$ and a set of *state variables* $\mathbf{u} := (u_1, u_2 \dots, u_m)$ satisfying state equations. For the classical minimum compliance problem, the objective function $\mathcal{J}$ is the compliance of a design where each $D_i$ corresponds to the region of $\Omega$ occupied by specific material (or void) and the state variable is the equilibrium displacement given as the solution of the static elasticity equations associated with the design $\mathbf{D}$ and a set of given loadings.

Unconstrained optimal design problems typically lead to trivial solutions, so one typically considers additional restrictions on the design or state variable. The most common class of constraints applies to the design variable, for instance, inclusions (*i.e.,* prescribing the material occupying specific regions of the domain), bounds on the volume fraction of each material, geometric features accounting for limitations of classical or additive manufacturing techniques. Constraints on the state variables include bounds on the maximum pointwise stress in the minimum compliance problem (Duysinx and Bendsøe 1998; Allaire et al. 2004; Lipton and Stuebner 2006; Allaire and Jouve 2008), or material non-linearities such as plasticity (Maute et al. 1998; Maury et al. 2018), fatigue Desmorat and Desmorat (2008), or fracture (Hsueh and Bhattacharya 2018; Li et al. 2021) for instance.

This article is concerned with the specific case where the state equations can be reformulated as a constrained optimization problem:

$$\min_{\mathbf{D}\in\mathbf{K}} \mathcal{J}(\mathbf{D}, \mathbf{u}) \tag{1a}$$

subject to

$$\mathbf{u} = \arg\min_{\mathbf{v}\in\mathbf{V}} \mathcal{E}(\mathbf{D}, \mathbf{v}), \tag{1b}$$

where $\mathbf{K}$ denotes the set of admissible designs and $\mathbf{V}$ the state of admissible states, $\mathcal{J}$ is the objective function and $\mathcal{E}$ is an energy from which the state equations can be derived.

When $\mathbf{V}$ is a subset of the natural space for the state variable, this class of problems is often referred to as Minimization Problems with Equilibrium Constraints (MPEC) (Luo

Responsible Editor: Gregoire Allaire

✉ Blaise Bourdin
bourdin@mcmaster.ca

[1] Department of Mathematics, Louisiana State University, Baton Rouge, LA 70803, USA

[2] Department of Mathematics & Statistics, McMaster University, Hamilton, ON, Canada

et al. 1996; Kočvara Outrata 1995; Outrata 1994; Outrata and Zowe 1995; Baumrucker et al. 2008; Maury et al. 2018). In this case, the first-order optimality conditions for (1b) take the form of the system of Karush–Kuhn–Tucker (KKT) conditions which can be written as variational inequalities of the first kind (Kinderlehrer and Stampacchia 2000), and the classical adjoint approach for PDE-constrained optimization cannot be applied directly. Instead, some authors have proposed to derive optimality conditions for MPEC problems in the sense of weak directional differentiability (Mignot and Puel 1984; Sokolowski and Zolesio 1992) for instance. Regularization and penalization methods are also often used (Drabla et al. 1998; Fukushima and Pang 1999; Scholtes 2001; Hu and Ralph 2004; Chouly 2013; Maury 2016; Maury et al. 2017, 2018). One drawback of these approaches is that enforcing the constraints typically requires very large penalty factors which can lead to numerical issues.

In this article, we introduce an active set approach for MPEC problems, which allows us to leverage standard adjoint methods without regularizing or penalizing the state constraint. We focus on a simple problem of compliance optimization under an obstacle problem similar to that studied in Haslinger and Klarbring (1993), but we believe that our approach is applicable to a wide range of situations where the state equations can be formulated as a minimization problem under inequality constraint, noticing that many problems in defect mechanics can be formulated this way, including damage (Francfort and Marigo 1993), brittle fracture (Francfort and Marigo 1998; Bourdin et al. 2008), or plasticity (Dal Maso et al. 2006; Babadjian et al. 2012).

Section 2 introduces the problem settings and our active set approach, after recalling some essential properties. Section 3 is devoted to a critical study of the performance and robustness of our approach, and comparison to classical penalization methods. Finally, Sect. 4 includes conclusions and perspectives.

## 2 A phase-field approach to optimal design with obstacle constraints

Consider the well-known minimum compliance problem with perimeter penalization, written in variational form (Ambrosio and Buttazzo 1993; Haber et al. 1996, see] [for instance):

$$\inf_{D\in\mathbf{K}}\left\{\mathcal{J}(D,\mathbf{u}) := \int_{\Gamma_N}\mathbf{g}\cdot\mathbf{u}\,\mathrm{dS} + \eta|D| + \kappa H^{n-1}(\partial D\cap\bar{\Omega})\right\} \tag{2a}$$

subject to

$$\mathbf{u} := \underset{\mathbf{v}\in\mathbf{V}}{\arg\min}\left\{\mathcal{E}(D,\mathbf{v}) = \int_\Omega \frac{1}{2}\varphi(D)\mathbf{A}e(\mathbf{v}) : e(\mathbf{v})\,\mathrm{d}\mathbf{x} - \int_{\Gamma_N}\mathbf{g}\cdot\mathbf{v}\,\mathrm{dS}\right\}. \tag{2b}$$

Here $D\subset\Omega$ denotes the design, *i.e.,* a region of a background domain $\bar{\Omega}$ occupied by a material with Hooke's law $\mathbf{A}$, where $\mathbf{A}$ is a symmetric tensor. $\mathbf{K} := \{\Omega_0\subset D\subset\bar{\Omega}\}$, and $\Omega_0$ denotes a region of $\Omega$ which must be contained in all designs. $\mathbf{u}$ is the elastic equilibrium displacement, $\varphi(D) = (1-\delta)\chi_D + \delta$, with $0<\delta\ll 1$ a small regularization parameter, and $\eta$ and $\kappa$ two positive constants. The prescribed boundary force $\mathbf{g}$ acting on a part $\Gamma_N$ of the boundary of $\Omega$ is assumed regular enough, and $H^{n-1}(\partial D\cap\bar{\Omega})$ is the $n-1$ dimensional measure of $\partial D$, *i.e.,* the perimeter of the design in 2D and its surface area in 3D. The natural space for admissible displacements is $\{\mathbf{u}\in H^1(\Omega;\mathbb{R}^n);\mathbf{u}=0 \text{ on } \Gamma_D\}$, with $\Gamma_D = \partial\Omega\setminus\Gamma_N$.

We add an additional obstacle constraint by further restricting the admissible displacements:

$$\mathbf{V} := \{\mathbf{u}\in H^1(\Omega;\mathbb{R}^n);\mathbf{u}=0 \text{ on } \Gamma_D,\ \tilde{\Omega}_i\subset\Omega+\mathbf{u}(\Omega)\subset\tilde{\Omega}_e\}, \tag{3}$$

where $\tilde{\Omega}_i$ and $\tilde{\Omega}_e$ are given obstacles (see Fig. 1). Note that owing to the injectivity of the displacement field, it is sufficient to enforce that $\partial\Omega+\mathbf{u}(\partial\Omega)\subset\tilde{\Omega}$. Furthermore, in the setting of small deformations, (3) can be reformulated as

$$\mathbf{V} := \{\mathbf{u}\in H^1(\Omega;\mathbb{R}^n);\mathbf{u}=0 \text{ on } \Gamma_D,\ u_i\le\mathbf{u}\cdot\mathbf{n}\le u_e \text{ on } \Gamma_N\}, \tag{4}$$

where $u_i$ and $u_e$ are given scalar functions and $\mathbf{n}$ is the outer normal to $\Omega$.

Following the phase-field approach devised in Bourdin and Chambolle (2003, 2006), we introduce a small regularization variable $\ell$ and a smooth function $\alpha$ taking its values

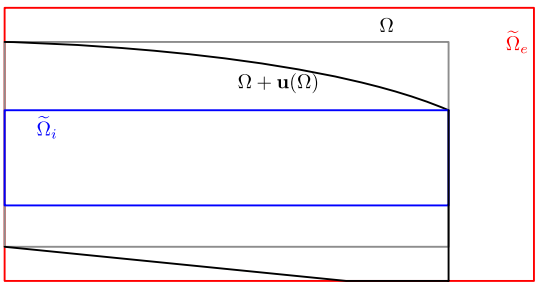


**Fig. 1** Obstacle problem. The background domain in the reference configuration is shown in gray and its deformed configuration is in black. The inner and outer obstacles $\tilde{\Omega}_i$ and $\tilde{\Omega}_e$ are shown in blue and red, respectively

in [0, 1] representing the domain $D$. The elastic energy becomes

$$\mathcal{E}_\ell(\alpha, \mathbf{u}) := \int_\Omega \frac{1}{2}\boldsymbol{\Phi}(\alpha)\mathbf{A}e(\mathbf{u}) \cdot e(\mathbf{u})\,\mathrm{d}\mathbf{x} - \int_{\Gamma_N} \mathbf{g} \cdot \mathbf{u}\,\mathrm{dS}, \tag{5}$$

where $\boldsymbol{\Phi}$ is a continuous differentiable monotonically increasing function with $\boldsymbol{\Phi}(0) = \delta$ and $\boldsymbol{\Phi}(1) = 1$. A typical choice is

$$\boldsymbol{\Phi}(\alpha) = (1 - \delta)\alpha^p + \delta, \tag{6}$$

where $p \geq 1$ is a given parameter. The perimeter penalty term $H^{n-1}(\partial D \cap \bar{\Omega})$ is approximated in the sense of $\Gamma$–convergence by

$$\mathcal{P}_\ell(\alpha) = \frac{1}{2c_W} \int_\Omega \frac{W(\alpha)}{\ell} + \ell|\nabla\alpha|^2\ \mathrm{d}\mathbf{x}, \tag{7}$$

where $W$ is a non-negative function vanishing only at 0 and 1, and $c_W := \int_0^1 \sqrt{W(t)}\,\mathrm{d}t$ is a normalization parameter (Braides 1998; Alberti 2000). Finally, the volume fraction of the design is approximated by $\int_\Omega \alpha^q\ \mathrm{d}x$, where $q \geq 1$ is a given parameter, so that the objective function becomes

$$\mathcal{J}_\ell(\alpha, \mathbf{u}) := \int_{\Gamma_N} \mathbf{g} \cdot \mathbf{u}\ \mathrm{dS} + \eta \int_\Omega \alpha^q\ \mathrm{d}\mathbf{x} + \kappa\mathcal{P}_\ell(\alpha). \tag{8}$$

The minimum compliance with obstacle constraints can therefore be reformulated as

$$\inf_{\alpha \in \mathbf{K}_\ell} \left\{\mathcal{J}_\ell(\alpha, \mathbf{u})\right\} \tag{9a}$$

subject to

$$\mathbf{u} := \arg\min_{\mathbf{v} \in \mathbf{V}} \left\{\mathcal{E}_\ell(\alpha, \mathbf{v})\right\}, \tag{9b}$$

where

$$\mathbf{K}_\ell := \left\{\rho \in H^1(\Omega;[0, 1]);\ \rho(\mathbf{x}) = 1 \text{ a.e. in } \Omega_0\right\}. \tag{10}$$

### 2.1 State equations in strong form

Given an admissible design $\alpha \in \mathbf{K}_\ell$, let $\mathbf{u} \in \mathbf{V}$ be the solution of the state equations. We define

$$\Gamma_i := \left\{\mathbf{x} \in \Gamma_N;\ \mathbf{u}(\mathbf{x}) \cdot \mathbf{n} = u_i(\mathbf{x})\right\}, \tag{11}$$

and

$$\Gamma_e := \left\{\mathbf{x} \in \Gamma_N;\ \mathbf{u}(\mathbf{x}) \cdot \mathbf{n} = u_e(\mathbf{x})\right\}. \tag{12}$$

Consider $\mathbf{v} \in H^1(\Omega;\mathbb{R}^n)$ such that $\mathbf{v} = 0$ on $\Gamma_D$, $\mathbf{v} \cdot \mathbf{n} \geq 0$ on $\Gamma_i$, and $\mathbf{v} \cdot \mathbf{n} \leq 0$ on $\Gamma_e$. For any $t \geq 0$, $\mathbf{u} + t\mathbf{v}$ is an admissible field for the state equations and

$$\mathcal{E}_\ell(\alpha, \mathbf{u} + t\mathbf{v}) - \mathcal{E}_\ell(\alpha, \mathbf{u}) \geq 0.$$

Sending $t$ to 0, we get that

$$\int_\Omega \boldsymbol{\Phi}(\alpha)\mathbf{A}e(\mathbf{u}) \cdot e(\mathbf{v})\,\mathrm{d}\mathbf{x} - \int_{\Gamma_N} \mathbf{g} \cdot \mathbf{v}\,\mathrm{dS} \geq 0,$$

and using Green's formula that

$$\begin{aligned} &- \int_\Omega \mathrm{div}[\boldsymbol{\Phi}(\alpha)\mathbf{A}e(\mathbf{u})] \cdot \mathbf{v}\,\mathrm{d}\mathbf{x} \\ &\quad + \int_{\Gamma_N} \boldsymbol{\Phi}(\alpha)\mathbf{A}e(\mathbf{u})\mathbf{n} \cdot \mathbf{v}\,\mathrm{dS} - \int_{\Gamma_N} \mathbf{g} \cdot \mathbf{v}\,\mathrm{dS} \geq 0. \end{aligned} \tag{13}$$

Considering first an arbitrary function $\mathbf{v}$ vanishing on $\Gamma_N$, and noticing that $-\mathbf{v}$ is also admissible, we quickly recover that $\mathrm{div}[\boldsymbol{\Phi}(\alpha)\mathbf{A}e(\mathbf{u})] = 0$ in $\Omega$, so that (13) becomes

$$\int_{\Gamma_N} \boldsymbol{\Phi}(\alpha)\mathbf{A}e(\mathbf{u})\mathbf{n} \cdot \mathbf{v}\,\mathrm{dS} - \int_{\Gamma_N} g \cdot \mathbf{v}\,\mathrm{dS} \geq 0.$$

Choosing then an arbitrary test function $\mathbf{v}$ vanishing on $\Gamma_i$ and $\Gamma_e$, and repeating the same derivation procedure, we get that

$$\boldsymbol{\Phi}(\alpha)\mathbf{A}e(\mathbf{u})\mathbf{n} = \mathbf{g} \text{ on } \Gamma_N \setminus \left(\Gamma_i \cup \Gamma_e\right).$$

Finally, consider a test function $\mathbf{v}$ and decompose its trace $\tilde{\mathbf{v}}$ on $\partial\Omega$ as $\tilde{\mathbf{v}} = (\tilde{\mathbf{v}} \cdot \mathbf{n})\mathbf{n} + (\tilde{\mathbf{v}} - (\tilde{\mathbf{v}} \cdot \mathbf{n})\mathbf{n})$. Using $\mathbf{v}$ and an extension of $(\tilde{\mathbf{v}} \cdot \mathbf{n})\mathbf{n} - (\tilde{\mathbf{v}} - (\tilde{\mathbf{v}} \cdot \mathbf{n})\mathbf{n})$ as test functions in (13), we obtain that

$$(\boldsymbol{\Phi}(\alpha)\mathbf{A}e(\mathbf{u})\mathbf{n} - \mathbf{g}) \cdot \mathbf{n} \geq 0 \text{ on } \Gamma_i,$$

and

$$(\boldsymbol{\Phi}(\alpha)\mathbf{A}e(\mathbf{u})\mathbf{n} - \mathbf{g})) \cdot \mathbf{n} \leq 0 \text{ on } \Gamma_e.$$

Putting everything together, we obtain the following first-order optimality conditions for the state equations:

$$\mathrm{div}[\boldsymbol{\Phi}(\alpha)\mathbf{A}e(\mathbf{u})] = 0 \text{ in } \Omega, \tag{14a}$$

$$(\boldsymbol{\Phi}(\alpha)\mathbf{A}e(\mathbf{u})\mathbf{n} - \mathbf{g}) \cdot \mathbf{n} \geq 0 \text{ on } \Gamma_i, \tag{14b}$$

$$\boldsymbol{\Phi}(\alpha)\mathbf{A}e(\mathbf{u})\mathbf{n} = \mathbf{g} \text{ on} \Gamma_N \setminus (\Gamma_i \cup \Gamma_e), \tag{14c}$$

$$(\boldsymbol{\Phi}(\alpha)\mathbf{A}e(\mathbf{u})\mathbf{n} - \mathbf{g}) \cdot \mathbf{n} \leq 0 \text{ on } \Gamma_e, \tag{14d}$$

$$\mathbf{u} = 0 \text{ on } \Gamma_D. \tag{14e}$$

### 2.2 Sensitivity analysis

In order to use a gradient or higher order method, one needs to compute the sensitivity of the objective function

with respect to design changes. Direct application of a the chain rule requires the sensitivity of the state variable with respect to the design variable. Because of the inequality constraints (14b) and (14d) on the state variable, the well-known adjoint method cannot be applied directly in our case. Instead, we define the following active sets:

$$\mathcal{I}_i := \{\mathbf{x} \in \Gamma_N;\, \mathbf{u}(\mathbf{x}) \cdot \mathbf{n} = u_i(\mathbf{x}), \\ (\boldsymbol{\Phi}(\alpha)\mathbf{A}e(\mathbf{u})\mathbf{n} - \mathbf{g}) \cdot \mathbf{n} \geq 0\}, \tag{15}$$

$$\mathcal{I}_e := \{\mathbf{x} \in \Gamma_N;\, \mathbf{u}(\mathbf{x}) \cdot \mathbf{n} = u_e(\mathbf{x}), \\ (\boldsymbol{\Phi}(\alpha)\mathbf{A}e(\mathbf{u})\mathbf{n} - \mathbf{g}) \cdot \mathbf{n} \leq 0\}, \tag{16}$$

and

$$\mathcal{I} := \mathcal{I}_i \cup \mathcal{I}_e. \tag{17}$$

Assuming that these active sets are known, the minimum compliance problem (9a–9b) can be rewritten as

$$\inf_{\alpha \in \mathbf{K}_\ell} \left\{ \mathcal{J}_\ell(\alpha, \mathbf{u}) \right\}$$

subject to

$$\operatorname{div}[\boldsymbol{\Phi}(\alpha)\mathbf{A}e(\mathbf{u})] = 0 \text{ in } \Omega, \tag{18a}$$

$$\boldsymbol{\Phi}(\alpha)\mathbf{A}e(\mathbf{u})\mathbf{n} = \mathbf{g} \text{ on } \Gamma_N \setminus \mathcal{I}, \tag{18b}$$

$$\mathbf{u} \cdot \mathbf{n} = \bar{u} \text{ on } \mathcal{I}, \tag{18c}$$

$$\mathbf{u} = 0 \text{ on } \Gamma_D, \tag{18d}$$

with

$$\bar{u} = \begin{cases} u_i & \text{on } \mathcal{I}_i, \\ u_e & \text{on } \mathcal{I}_e. \end{cases}$$

As all inequality constraints have been replaced with equality constraints (again, assuming the knowledge of the active sets $\mathcal{I}_i$ and $\mathcal{I}_e$), we can follow the classical adjoint approach to the computation of the sensitivity of the objective function. Let $\lambda \in H^1(\Omega;\mathbb{R}^n)$ such that $\lambda = 0$ on $\Gamma_D \cup \mathcal{I}$ be the Lagrange multiplier associated to the constraints (18a–18d). We introduce the Lagrangian

$$\mathcal{L}(\alpha, \mathbf{u}, \boldsymbol{\lambda}) = \int_{\Gamma_N} \mathbf{g} \cdot \mathbf{u} \, \mathrm{dS} + \eta \int_\Omega \alpha^q \, \mathrm{d}\mathbf{x} + \kappa \mathcal{P}_\ell(\alpha) \\ - \int_\Omega \boldsymbol{\lambda} \cdot \operatorname{div}[\boldsymbol{\Phi}(\alpha)\mathbf{A}e(\mathbf{u})] \, \mathrm{d}\mathbf{x}. \tag{19}$$

Using Green's formula, we get that

$$\mathcal{L}(\alpha, \mathbf{u}, \boldsymbol{\lambda}) = \int_{\Gamma_N} \mathbf{g} \cdot (\mathbf{u} - \lambda) \, \mathrm{dS} + \eta \int_\Omega \alpha^q \, \mathrm{d}\mathbf{x} + \kappa \mathcal{P}_\ell(\alpha) \\ + \int_\Omega \boldsymbol{\Phi}(\alpha)\mathbf{A}e(\mathbf{u}) \cdot e(\boldsymbol{\lambda}) \, \mathrm{d}\mathbf{x}. \tag{20}$$

Note that if $\mathbf{u}$ satisfies the state equations (18a–18d), then $\mathcal{L}(\alpha, \mathbf{u}, \boldsymbol{\lambda}) = \mathcal{J}_\ell(\alpha, \mathbf{u})$, so that computing the Fréchet derivative of $\mathcal{J}_\ell$ associated with a design change $\gamma$ is equivalent to computing that of $\mathcal{L}$:

$$\mathcal{D}\mathcal{J}_\ell(\alpha, \mathbf{u})(\gamma) = \mathcal{D}\mathcal{L}(\alpha, \mathbf{u}, \boldsymbol{\lambda})(\gamma) \tag{21}$$

$$= \left\langle \frac{\partial \mathcal{L}(\alpha, \mathbf{u}, \boldsymbol{\lambda})}{\partial \alpha}, \gamma \right\rangle + \left\langle \frac{\partial \mathcal{L}(\alpha, \mathbf{u}, \boldsymbol{\lambda})}{\partial \mathbf{u}}, \frac{\partial \mathbf{u}}{\partial \alpha}\gamma \right\rangle \\ + \left\langle \frac{\partial \mathcal{L}(\alpha, \mathbf{u}, \boldsymbol{\lambda})}{\partial \lambda}, \frac{\partial \lambda}{\partial \alpha}\gamma \right\rangle. \tag{22}$$

As a result of choosing Lagrange multiplier $\lambda$, the last term in Equation (22) disappears. In addition, computing $\frac{\partial \mathbf{u}}{\partial \alpha}$ is typically difficult. Instead, we search for $\lambda$ such that for any $\mathbf{v} \in H^1(\Omega)$ with $\mathbf{v} = 0$ on $\Gamma_D \cup \mathcal{I}$,

$$\left\langle \frac{\partial \mathcal{L}(\alpha, \mathbf{u}, \boldsymbol{\lambda})(\gamma)}{\partial \mathbf{u}}, \mathbf{v} \right\rangle = \int_{\Gamma_N \setminus \mathcal{I}} [\boldsymbol{\Phi}(\alpha)\mathbf{A}e(\boldsymbol{\lambda})\mathbf{n} + \mathbf{g}] \cdot \mathbf{v} \, \mathrm{dS} \\ - \int_\Omega \operatorname{div}[\boldsymbol{\Phi}(\alpha)\mathbf{A}e(\boldsymbol{\lambda})] \cdot \mathbf{v} \, \mathrm{d}\mathbf{x} = 0. \tag{23}$$

Equation (23) is usually referred to as the adjoint equation associated with the constraints, and given any solution $\lambda$, then obtain

$$\mathcal{D}\mathcal{J}_\ell(\alpha, \mathbf{u})(\gamma) = \left\langle \frac{\partial \mathcal{L}(\alpha, \mathbf{u}, \boldsymbol{\lambda})}{\partial \alpha}, \gamma \right\rangle \\ = \eta q \int_\Omega \alpha^{q-1}\gamma \, \mathrm{d}\mathbf{x} + \frac{\kappa}{2c_W} \int_\Omega \frac{W'(\alpha)}{\ell}\gamma + 2\ell \nabla\alpha \cdot \nabla\gamma \, \mathrm{d}\mathbf{x} \\ + \int_\Omega \boldsymbol{\Phi}'(\alpha)\mathbf{A}e(\mathbf{u}) \cdot e(\boldsymbol{\lambda})\gamma \, \mathrm{d}\mathbf{x}. \tag{24}$$

***Remark 1*** Note that (23) can be written in strong form as

$$\begin{cases} -\operatorname{div}[\boldsymbol{\Phi}(\alpha)\mathbf{A}e(\boldsymbol{\lambda})] = 0 & \text{in } \Omega, \\ \boldsymbol{\Phi}(\alpha)\mathbf{A}e(\boldsymbol{\lambda})\mathbf{n} = -\mathbf{g} & \text{on } \Gamma_N \setminus \mathcal{I}, \\ \boldsymbol{\lambda} = 0 & \text{on } \Gamma_D \cup \mathcal{I}. \end{cases} \tag{25}$$

so that if neither of the obstacle constraints are active, *i.e.*, when $\mathcal{I} = \mathcal{I}_i = \mathcal{I}_e = \emptyset$, we recover the classical result $\boldsymbol{\lambda} = -\mathbf{u}$.

#### 2.2.1 Numerical implementation

Our numerical implementation uses FEniCS, a collection of open-source projects for the solution of partial differential equations using a high-level description of the variational forms involved (Alnæs et al. 2014, 2015; Alnæs 2012; Alnæs et al. 2009, 2012; Kirby 2004, 2012), (Kirby and Logg 2006; Logg et al. 2012, 2012b; Logg and Wells 2010; Logg et al. 2012c; Mitusch et al. 2019; Ølgaard and Wells 2010), and the TAO optimization package, now part of PETSc (Balay et al. 1997, 2021b, a). In all that follows, all fields are discretized using linear and quadratic Lagrange simplicial finite elements. We limited our implementation to rectangular domain so that the obstacle constraints become simple box constraints on the state variable, and use the BLMVM (bound limited-memory, variable-metric) algorithm of TAO, which requires the objective function and its gradient only.

Note that (24) assume that the active sets are known *a priori*, which is of course not the case. Instead, we use PETSc's variational inequality solvers (SNESVI) to solve the state equations every time we need to evaluate the objective function, and update the active sets. A classical approach is to introduce a large number $c \gg 0$, typically $c = 10^8$, and define

$$g_i := \frac{\partial \mathcal{E}_\ell}{\partial \mathbf{u}}(\alpha, \mathbf{u}) \cdot \mathbf{n} + c(u_i - \mathbf{u} \cdot \mathbf{n}) \tag{26}$$

and

$$g_e := \frac{\partial \mathcal{E}_\ell}{\partial \mathbf{u}}(\alpha, \mathbf{u}) \cdot \mathbf{n} + c(u_e - \mathbf{u} \cdot \mathbf{n}), \tag{27}$$

$\frac{\partial \mathcal{E}_\ell}{\partial \mathbf{u}}$ denoting the Fréchet derivative of the elastic energy $\mathcal{E}_\ell$ with respect to $\mathbf{u}$. If $g_i(\mathbf{x})$ is strictly positive for some $\mathbf{x}$ on $\Gamma_N$, then $\mathbf{x}$ belongs to the active set $\mathcal{I}_i$ associated to the lower bound. Similarly, a point $\mathbf{x}$ on $\Gamma_N$ at which $g_e(\mathbf{x})$ is strictly negative belongs to the active set $\mathcal{I}_e$ associated to the upper bound. An alternative is to derive $\mathcal{I}$ from the Jacobian of the state equations, if available in the solvers used. In practice, we found it sufficient to determine the active sets as the degree of freedom at which the displacement reaches obstacles and ignore the sign of the reaction force (the second terms in (15–16)).

***Remark 2*** Given a design $\alpha$, evaluating the objective function requires recomputing the state and adjoint variables, which is computationally intensive, while the computation of its gradient is simple in comparison. In the context of an optimization algorithm, this means that the computational cost of a line search can be high. The BLMVM algorithm uses a line search (Moré and Thuente 1994) which typically converges in a few iterations. We have not tried to optimize this part of the algorithm, or studied the impact of the accuracy of the line search on the overall computational efficiency of our approach.

## 3 Numerical results

We present a series of numerical simulations illustrating the strengths of our approach. In all that follows, we consider a two-dimensional rectangular domain $\Omega$ with width $L_x = 1$ and height $L_y = 0.3$ in plane stress conditions. We use the double-well function $W(s) := s(1-s)$ in (7), hence $c_W = \int_0^1 \sqrt{W(t)}\, dt = \pi/8$. The structural material is assumed isotropic with Young's modulus $E = 10^3$ Pa and Poison ratio $\nu = 0.3$. We set $p = 2$, $q = 1$, and $\delta = 10^{-3}$ in (6) and (8). All computations were performed on 8 cores of a dual socket Intel Xeon X5677 at 3.47 GHz workstation.

### 3.1 Compliance optimization without obstacles

We start with the simplest case of an optimal design without obstacles described in Fig. 2.

A uniformly distributed traction force $\mathbf{g} = (0, -1)$ is applied on a part of the boundary $\Gamma_{N_T}$ of the domain $\Omega$, where $(x, y) \in \Omega$ and $5/6 \le x \le 1$ and $y = L_y$. On the boundary $\Gamma_{N_R}$, the displacement $\mathbf{u}$ in the $x$-direction is fixed. In addition, the left boundary $\Gamma_D$ is clamped in both $x$-direction and $y$-direction (see Fig. 2). The inner and outer obstacles are set respectively to a very small and very large value so that they are not active.

The domain is discretized with a structured mesh with cell size $h = 0.005$, consisting of 48,000 triangular finite elements. The regularization parameter is $\ell = 0.025$, the perimeter penalization parameter is $\kappa = \frac{5\pi}{8} \times 10^{-5}$, and the volume penalization parameter $\eta = 0.08$. The initial density field was chosen constant with value 1. The tolerance on the gradient of the objective function was set to $5 \times 10^{-8}$ in both approaches.

Note that as highlighted in Remark 1, in this case, the minimum compliance problem becomes self-adjoint. We

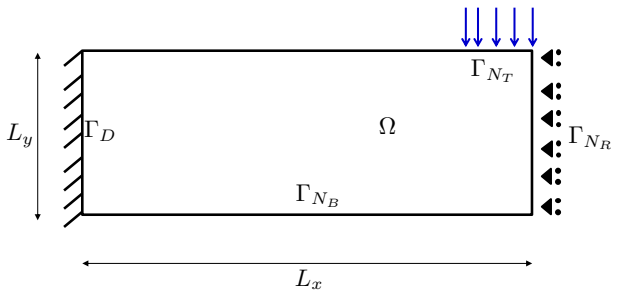


**Fig. 2** An optimization problem without obstacles

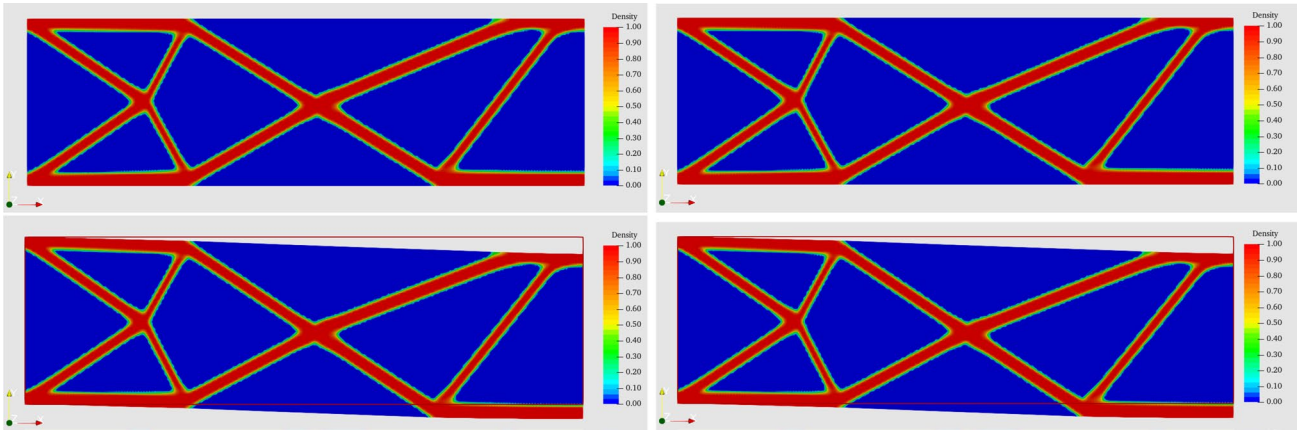

**Fig. 3** Optimal design without obstacle. Designs produced by the proposed approach (left column) and a penalization approach (right column) in the reference (top row) and deformed (bottom row)

did not modify our algorithm to account for the fact that the computation of the adjoint state is technically not necessary. Because solving the state and adjoint equations is the most computationally intensive part of the algorithm, the times reported below could therefore be significantly reduced.

For this problem, our algorithm attained the desired tolerance in 986 iterations (leading to 1,375 evaluations of the objective function) and 92 minutes. We compared our result to that obtained with the penalization approach implemented in the open-source code dolfin-adjoint (Farrell et al. 2013; Mitusch et al. 2019), described in Appendix A. This approach differs from ours in that the constraints on the state variables are enforced through a penalty term, adjusted during iterations. The penalization approach converged in 1019 iterations, with 1039 evaluations of the objective function, and 74 min. Note that a one-to-one comparison of the number of iterations of both methods is not directly significant as the penalization approach gradually solves the direct and adjoint problems for decreasing values of the penalty factor, $\epsilon$, from $10^{-4}$ to $6.25 \times 10^{-6}$. Despite the lack of uniqueness caused but the non-convexity of the cost function, both approaches lead to essentially identical designs (see Fig. 3). In the active set method the objective function decreased from $2.51948 \times 10^{-2}$ to $1.03486392 \times 10^{-2}$ vs. $2.51948 \times 10^{-2}$ to $1.03491319 \times 10^{-2}$ in the penalization approach.

## 3.2 Compliance optimization with a single obstacle

In a second example, we apply a uniform distributed traction force, $\mathbf{g} = (0, -1)$ and prescribe the value of the density function to 1 on part of the boundary $\Gamma_{N_T}$. Again the displacement $\mathbf{u}$ in the $x$-direction is fixed on the boundary $\Gamma_{N_R}$, and the left boundary $\Gamma_D$ is clamped in both

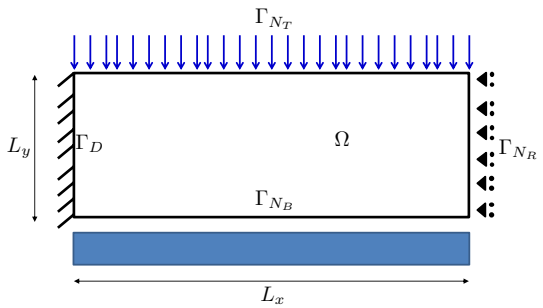


**Fig. 4** A problem with one obstacle

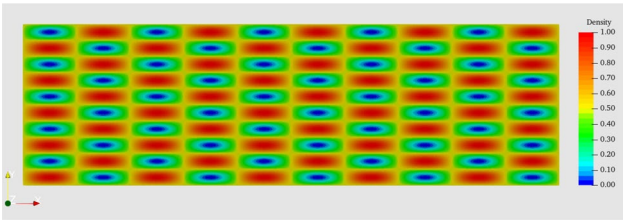

**Fig. 5** Initial guess $\alpha_0 = \frac{1}{2} + \frac{1}{2}\sin\left(\frac{10\pi x}{L_x}\right)\sin\left(\frac{10\pi y}{L_y}\right)$

$x$-direction and $y$-direction. The upper bound is set to be very large $u_{e_1}(\mathbf{x}) = \infty$ and the lower bound on $\Gamma_{N_B}$ is $u_{e_2}(\mathbf{x}) = -0.02 - y$.

In Fig. 4, the obstacle is shown as a blue box, and the blue arrows represent the traction force. The initial design, shown in Fig. 5, is

$$\alpha_0 = \frac{1}{2} + \frac{1}{2}\sin\left(\frac{10\pi x}{L_x}\right)\sin\left(\frac{10\pi y}{L_y}\right).$$

Using the same values of $\epsilon$ as above, the penalization method converged in 383.88 minutes after 3,028 iterations with 3,436 evaluations of the objective function while our approach converged in only 72.31 minutes and 886 iterations which required solving the state and adjoint equations 1,010 times. Results are shown in the reference and deformed configuration in Fig. 6. The obstacle is represented by a black line in the deformed configuration. The displacement field in the $y$-direction along the line $y = 0$ obtained by the active set and penalization method are shown as the red and black lines in Fig. 7, respectively. We observe that obstacle constraints on the displacement are satisfied exactly by the solution generated by the active set approach, from around $x = 0.6$ to $x = 1$ on $\Gamma_{N_B}$ but not by that of the penalization approach. Even though the constraint is satisfied exactly in our approach, so that the set of admissible designs is smaller, the final value of the objective function is smaller ($2.04956574 \times 10^{-2}$ in our approach vs. $2.57722763 \times 10^{-2}$ with the penalization approach).

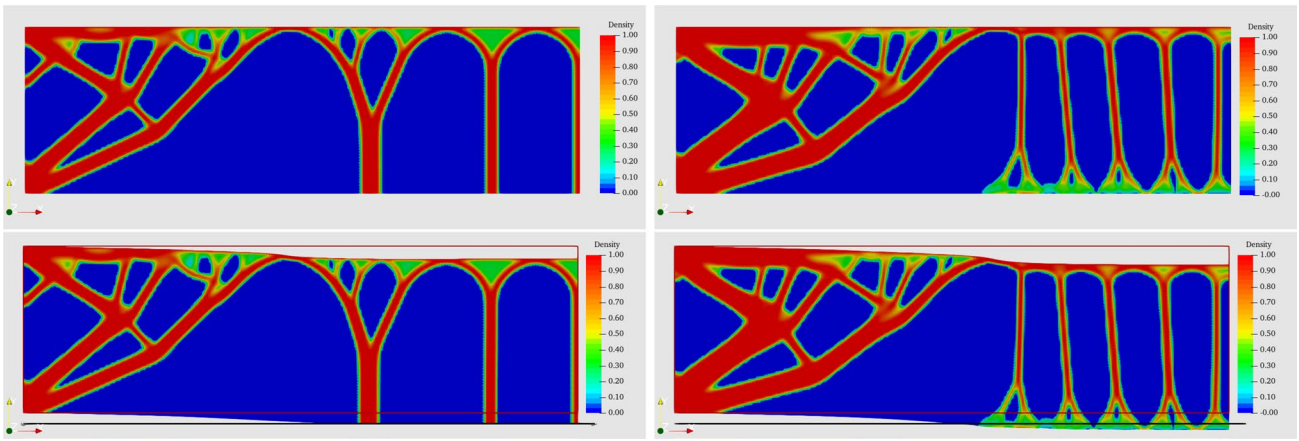

**Fig. 6** Optimal designs with one obstacle. Designs produced by the proposed approach (left column) and a penalization approach (right column) in the reference (top row) and deformed (bottom row) configurations. Note that the penalization approach produces a design that does not satisfy the obstacle constraint (represented by a black line)

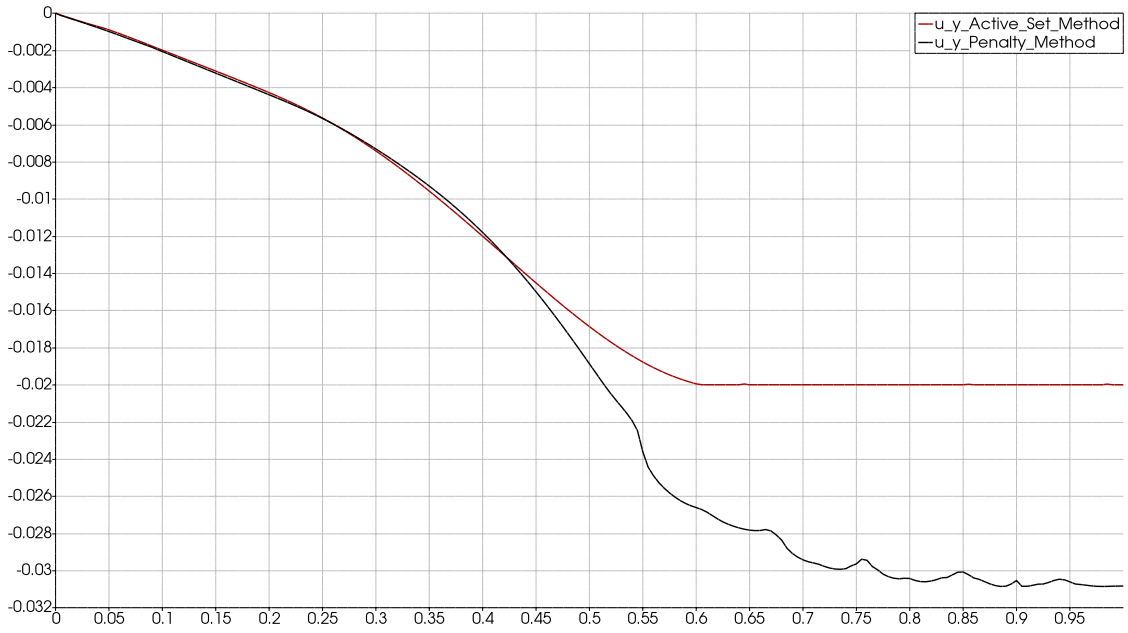


**Fig. 7** Vertical displacement of along the boundary $\Gamma_{N_B}$. The active set approach (shown in red) produces a design that satisfies the obstacle constraint exactly whereas the penalization approach (the black line) does not

### 3.2.1 Robustness of the active set approach

While filtering techniques (Bourdin 2001) or perimeter penalization (Ambrosio and Buttazzo 1993) can be used to ensure the well-posedness of optimal design problems, mesh independency is hard to achieve, owing in particular to the non-convexity of the optimization problems.

In order to demonstrate the robustness of our approach, we conducted series of computations on structured and unstructured meshes with decreasing element size. The unstructured meshes will be generated automatically by the FEniCS component mshr, based on CGAL and Tetgen (Si 2015), while the structured meshes were built by subdividing each cell of a Cartesian grid into four triangles as shown in Fig. 8.

The initial design was set to $\alpha_0 = \frac{1}{2} + \frac{1}{2}\sin(\frac{n\pi x}{L_x})\sin(\frac{n\pi y}{L_y})$, and the tolerance on the gradient of the objective function was set to $5 \times 10^{-8}$. Figure 9 shows the value of the objective function upon convergence for as a function of the mesh size varying varies from $4.33 \times 10^{-3}$ to $6.31 \times 10^{-3}$ for $n = 2$, 8, 10, and Fig. 10 shows some of the associated designs. We observe that structured meshes typically lead to smaller values of the objective function at convergence, and that while different initial guesses may lead to different designs, the actual values of the objective function are very close (see the range of $y$–values in Fig. 9).

Fig. 11 shows the final designs for structured meshes with $h_{\min} = 5 \times 10^{-3}$ and different initial guesses of the form $\alpha_0 = \frac{1}{2} + \frac{1}{2}\sin(\frac{n\pi x}{L_x})\sin(\frac{n\pi y}{L_y})$ with $n = 2$, $n = 4$, and $n = 8$. The values of the objective function are $2.04855932 \times 10^{-2}$, $2.05590338 \times 10^{-2}$, and $2.04849720 \times 10^{-2}$, respectively. Again, despite some minor differences in the actual designs, the variations of the objective function are only approximately 0.36%.

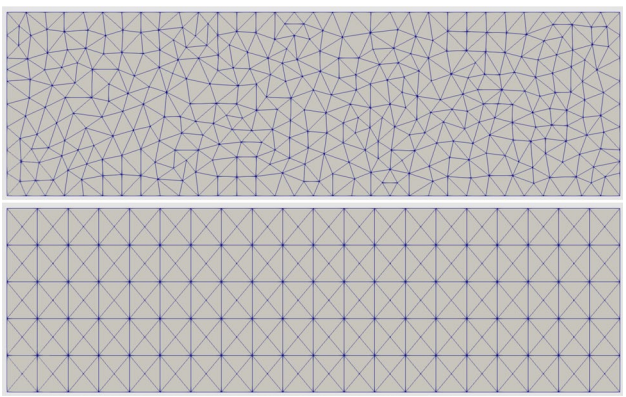

**Fig. 8** Typical unstructured and structured meshes

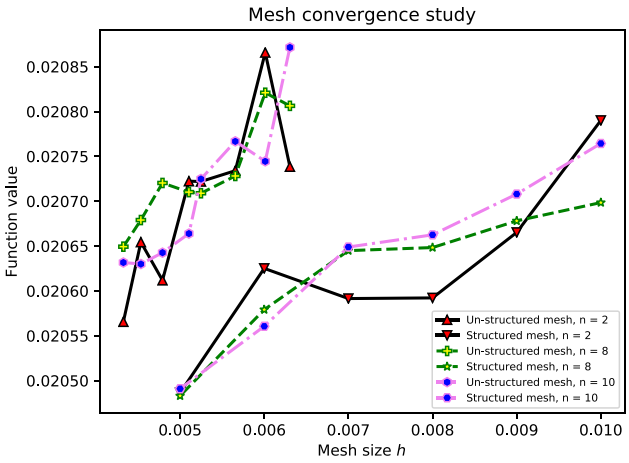


**Fig. 9** Convergence plot by the active set method with different mesh types and sizes

### 3.2.2 Sensitivity upon the perimeter penalty term $\kappa$

Since un-penalized problems are ill-posed, it is natural to expect that the penalty term on the perimeter $\kappa$ has a more significant impact on the designs. Figure 13 shows designs obtained with extreme values $\kappa = \pi \times 10^{-4}$ and $\kappa = \frac{\pi}{8} \times 10^{-15}$. All other parameters are kept as in the previous examples. As expected, a large weight on the perimeter leads to a very simple design whose complexity increases as $\kappa$ decreases. Figure 12 shows the evolution of the whole objective function, the compliance, and the perimeter penalty as a function of $\kappa$. Surprisingly, one observes that values of $\kappa$ as small as $\frac{\pi}{8} \times 10^{-15}$ produced well-defined designs exempt of large areas with intermediate density or checkerboard patterns.

## 3.3 Compliance optimization with two obstacles

Consider a problem involving two obstacles $u_1(\mathbf{x}) = -0.035 - y$ on $\Gamma_{N_B} := (0.4, 0.6) \times \{0\}$ and $u_2(\mathbf{x}) = 0.25 - y$ on $\Gamma_{N_T} := (0.1, 0.3) \times \{L_y\}$, and a downward force $\mathbf{g} := (0, -10)$ on $\Gamma_{N_R} := \{L_x\} \times \left(\frac{L_y}{3}, \frac{2L_y}{3}\right)$ while the horizontal displacement on the right edge is blocked (see Fig. 14 for a schematic representation of the load and obstacles). The first obstacle infringes upon the reference configuration and is therefore expected to be active. All of the materials, solvers, and model parameters are kept as in the previous examples with the exception of the volume penalization parameter $\eta$, which is set to 0.3. The initial guess for the density field is $\alpha_0 = \frac{1}{2} + \frac{1}{2}\sin\left(\frac{2\pi x}{L_x}\right)\sin\left(\frac{2\pi y}{L_y}\right)$ (see Fig. 15).

The design produced by our active set algorithm is shown in Fig. 16 in the reference and deformed configuration. Convergence was attained in 1,532 iterations

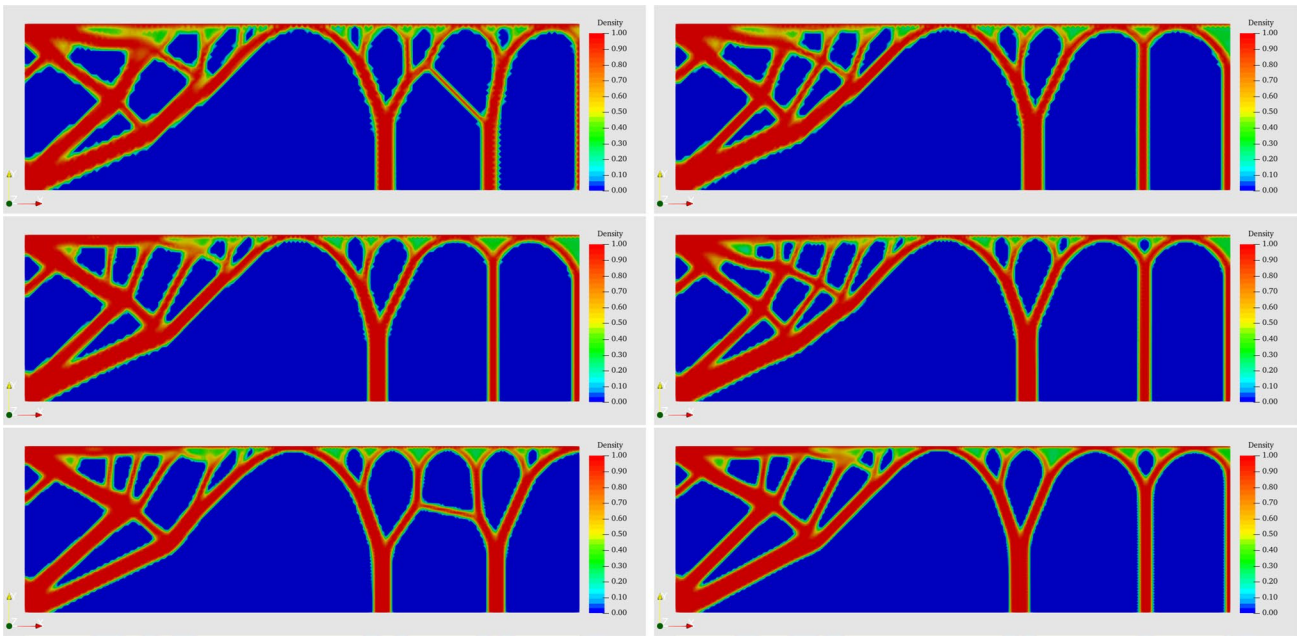

**Fig. 10** Structured mesh results with different minimum mesh size, $h_{\min} = 10^{-2}$, $9 \times 10^{-3}$, $8 \times 10^{-3}$, $7 \times 10^{-3}$, $6 \times 10^{-3}$, and $5 \times 10^{-3}$, and $n = 2$

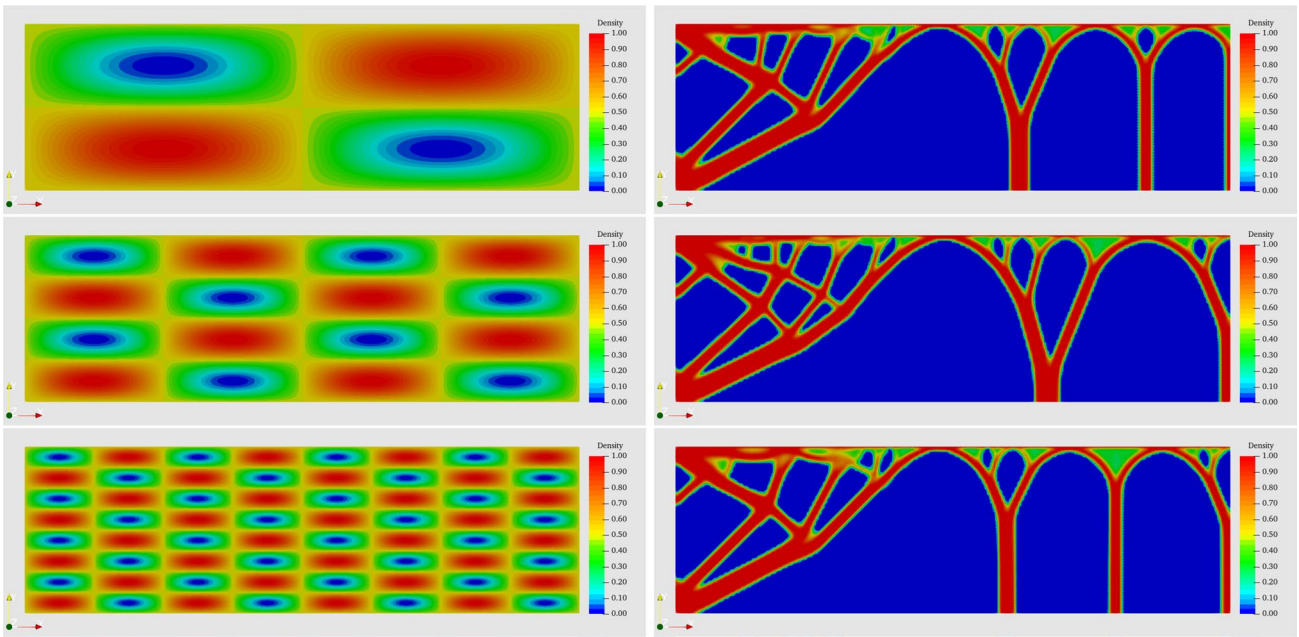

**Fig. 11** Initial guesses and the corresponding designs for $\alpha_0 = \frac{1}{2} + \frac{1}{2}\sin(\frac{2\pi}{L_x})\sin(\frac{2\pi}{L_y})$ (first row), $\alpha_0 = \frac{1}{2} + \frac{1}{2}\sin(\frac{4\pi}{L_x})\sin(\frac{4\pi}{L_y})$ (second row), and $\alpha_0 = \frac{1}{2} + \frac{1}{2}\sin(\frac{8\pi}{L_x})\sin(\frac{8\pi}{L_y})$ (third row)

and 124 minutes, with 1,828 evaluations of the state and adjoint equations. The objective function decreased smoothly from $15.0867 \times 10^{-2}$ to $1.98317590 \times 10^{-2}$. Our design is reminiscent of a compliant mechanism using the obstacles to provide mechanical advantage. The penalization approach converged to a tolerance of $5 \times 10^{-8}$ in 566 iterations and 175 minutes to a design that does not satisfy the upper obstacle constraint, shown in Fig. 16 (bottom row).

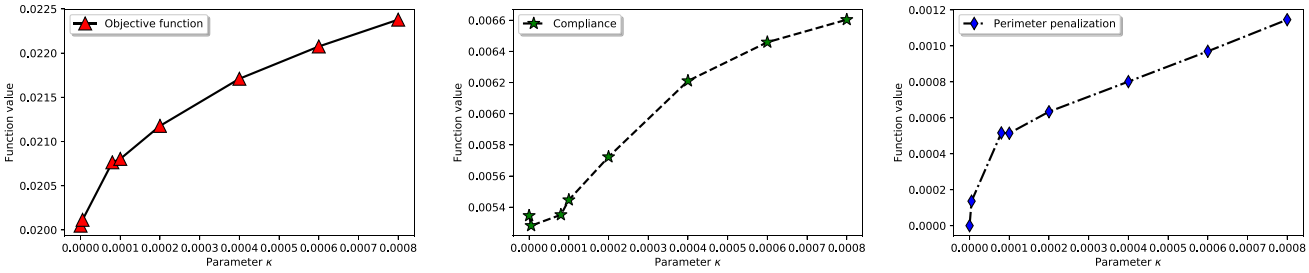


**Fig. 12** Influence the parameter $\kappa$. (left): objective function. (center): compliance. (right): perimeter penalization

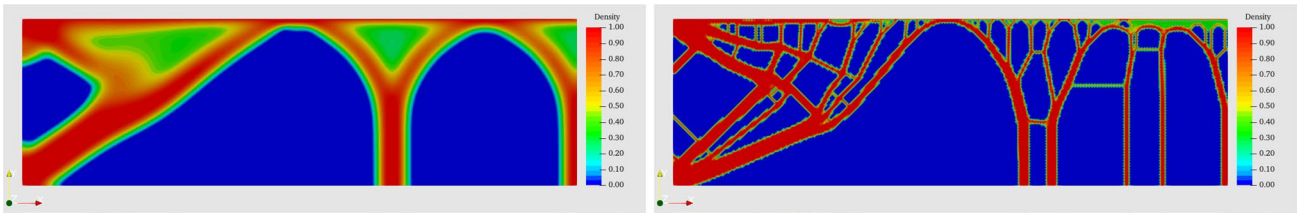


**Fig. 13** Influence of the parameter $\kappa$. (left): $\kappa = 8 \times 10^{-4}$. (right): $\kappa = 10^{-15}$

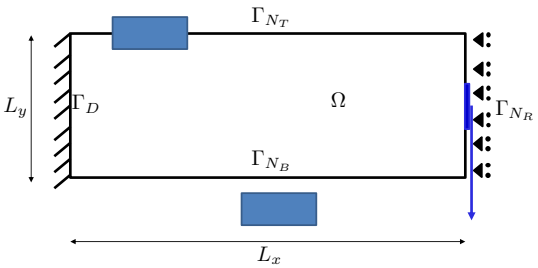


**Fig. 14** A problem with two obstacles

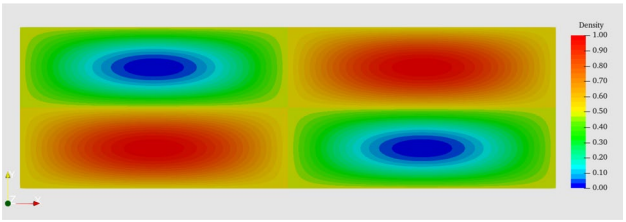


**Fig. 15** Initial guess $\alpha_0 = \frac{1}{2} + \frac{1}{2} \sin\left(\frac{2\pi x}{L_x}\right) \sin\left(\frac{2\pi y}{L_y}\right)$

As expected, increasing the weight penalty factor $\eta$ leads to lighter designs shown in Fig. 17. Our active set method converges again toward a design that satisfies both constraints. It uses the obstacles to provide mechanical advantage, but the additional penalty on the weight term leads to a design that does not make contact with the left edge of the domain. Here again, the penalization method fails to provide a design satisfying both constraints.

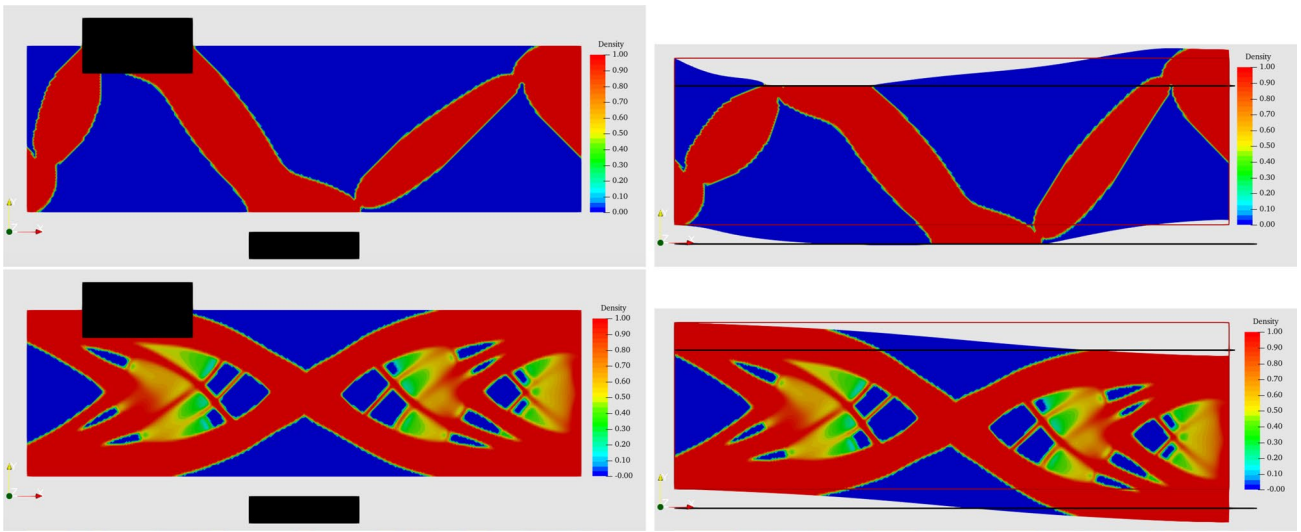

**Fig. 16** Optimal designs of a cantilever beam with two obstacles in the reference and deformed configurations, $\eta = 0.3$. Top row: active set method, bottom row: penalization method

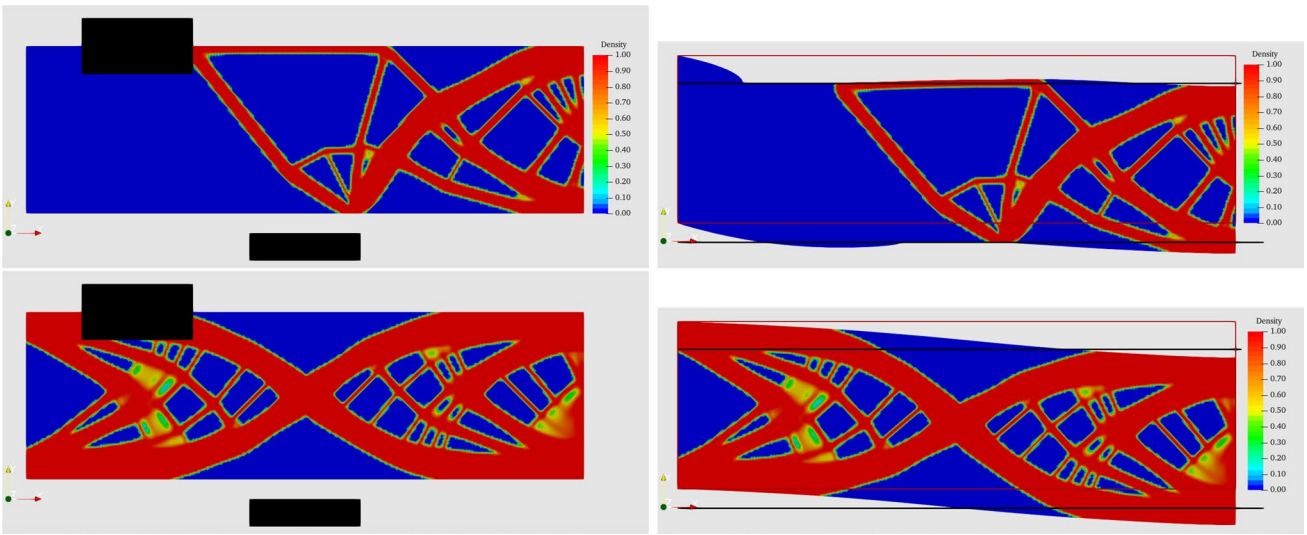

**Fig. 17** Optimal designs of a cantilever beam with two obstacles in the reference and deformed configurations, $\eta = 0.35$. Top row: active set method, bottom row: penalization method

## 4 Discussion and conclusion

The proposed active set method performed similarly to a classical penalization method for nonlinear optimization without obstacles. In the general case, however, our active set method is faster and more robust than the penalization approach and produces designs with smaller objective values. Furthermore, in the active set approach, the obstacle constraints are always satisfied, whereas penalization methods require a careful adjustment of the penalty terms and may not always lead to design satisfying the constraints on the state variable.

In addition, our approach exhibits good robustness properties upon mesh refinement or changes of initial design. In all fairness, it can produce slightly different designs for different initial designs, which is common in non-convex optimization problems, but the objective value of the computed designs are very close.

## Appendix: The penalization method

In order to use an adjoint-based method to compute the sensitivity of the objective function subject to the variational inequality (14a-14e), one can approximate the variational inequality by a family of nonlinear boundary value problems. For the sake of simplicity, we restrict the exposition to a lower bound on each component of the state variable $u_i \geq 0$ on $\Omega$, $i = 1, 2$.

Following the work of (Hintermüller and Kopacka 2011), let $\pi$ be the component-wise max operator

$$\pi(\mathbf{u}_\epsilon) : -\max(0, -\mathbf{u}_\epsilon), \quad \forall \mathbf{u}_\epsilon \in \mathbf{K}. \tag{28}$$

For any given $\alpha \in \mathbf{K}$ and for $\epsilon > 0$, consider the problem

$(\mathcal{Q}_\epsilon)$ : Find $\mathbf{u}_\epsilon \in \mathbf{K}$ such that

$$\int_\Omega \phi(\alpha)\mathbf{A}e(\mathbf{u}) \cdot e(\mathbf{v})\, \mathrm{d}\mathbf{x} + \frac{1}{\epsilon}\langle \pi(\mathbf{u}_\epsilon), \mathbf{v}\rangle = \langle T, \mathbf{v}\rangle, \tag{29}$$

for any appropriate test function $\mathbf{v}$. While, it is reasonable to expect that the solution of $(\mathcal{Q}_\epsilon)$ converge to the state equations as $\epsilon \to 0$, the analysis of the implementation of $(\mathcal{Q}_\epsilon)$ is rendered difficult by the lack of smoothness of the max function. Instead, one can replace $\pi$ by the smooth-max operator

$$\max_\epsilon(0, x) : \begin{cases} x - \frac{\epsilon}{2} & \text{if } x \geq \epsilon, \\ \frac{x^2}{2\epsilon} & \text{if } 0 < x < \epsilon, \\ 0 & \text{if } x \leq 0, \end{cases} \tag{30}$$

and define $(\mathcal{Q}'_\epsilon)$ : Find $\mathbf{u}_\epsilon \in \mathbf{K}$ such that

$$\int_\Omega \phi(\alpha)\mathbf{A}e(\mathbf{u}) \cdot e(\mathbf{v})\, \mathrm{d}\mathbf{x} + \frac{1}{\epsilon}\langle \pi_\epsilon(\mathbf{u}_\epsilon), \mathbf{v}\rangle = \langle T, \mathbf{v}\rangle, \tag{31}$$

for any appropriate test function $\mathbf{v}$.

Figure 18 shows the max and smooth-max functions with $\epsilon = 0.05$. Because $\pi_\epsilon : \mathbf{V} \longrightarrow \mathbf{V}^*$ is be continuous and monotone and the penalized problem $(\mathcal{Q}'_\epsilon)$ admits a unique solution. As $\epsilon \to 0$, $\pi(\mathbf{u}_\epsilon) \to 0$ , and the solution of $(\mathcal{Q}'_\epsilon)$, converges to the solution of the variational inequality (14a–14e). This approach is implemented in the open-source code dolfin-adjoint (Farrell et al. 2013; Mitusch et al. 2019), which we used as our reference implementation.

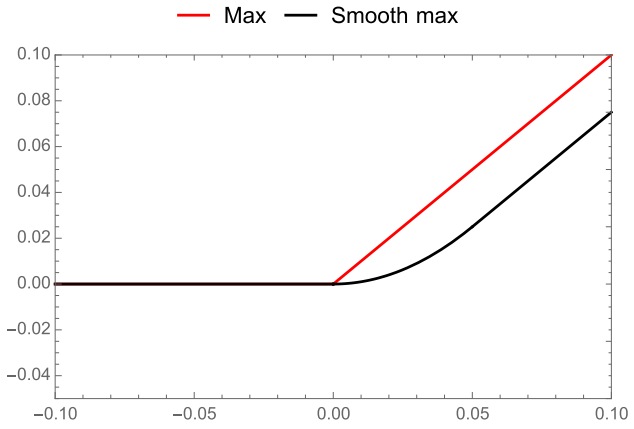


**Fig. 18** Max and smooth-max functions

**Acknowledgements** We gratefully acknowledge the support of the US National Science Foundation through Award no. DMS-1535083 and DMS-1535076 under the Designing Materials to Revolutionize and Engineer our Future (DMREF) Program. Portions of this research were conducted with high-performance computational resources provided by Louisiana State University (http://www.hpc.lsu.edu) and the Louisiana Optical Network Infrastructure (http://www.loni.org)Part of this work was performed while BB was the A.K. & Shirley Barton Professor of Mathematics at Louisiana State University (USA)

## Declarations

**Conflict of interest** The authors declare that they have no conflict of interest.

**Replication of results** The source code (Tran 2021) for the numerical simulations, as well as instructions required to reproduce all examples, is available at https://github.com/NhaVanTran/Optimal_Design_Active_Set_Approach.

## References

Alberti G (2000) Variational models for phase transitions, an approach via Γ-convergence. In: Buttazzo G, Marino M, Murthy MKV (eds) Calculus of variations and partial differential equations. Springer, New York, pp 95–114

Allaire G, Jouve F (2008) Minimum stress optimal design with the level set method. Eng Anal Boundary Elem 32(11):909–918. https://doi.org/10.1016/j.enganabound.2007.05.007

Allaire G, Jouve F, Maillot H (2004) Topology optimization for minimum stress design with the homogenization method. Struct Multidiscip Optim 28(2–3):87–98. https://doi.org/10.1007/S00158-004-0442-8

Alnæs M, Blechta J, Hake J, Johansson A, Kehlet B, Logg A, Richardson C, Ring J, Rognes ME, Wells GN (2015) The FEniCS project version 1.5. Arch Numer Softw 3(100):9–23

Alnæs MS (2012) UFL: a finite element form language. In: Automated solution of differential equations by the finite element method. Springer, New York, pp 303–338. https://doi.org/10.1007/978-3-642-23099-8_17

Alnæs MS, Logg A, Mardal KA, Skavhaug O, Langtangen HP (2009) Unified framework for finite element assembly. Int J Comput Sci Eng 4(4):231–244. https://doi.org/10.1504/IJCSE.2009.029160

Alnæs MS, Logg A, Mardal KA (2012) UFC: a finite element code generation interface. In: Automated solution of differential equations by the finite element method. Springer, New York, pp 283–302. https://doi.org/10.1007/978-3-642-23099-8_16

Alnæs MS, Logg A, Ølgaard KB, Rognes ME, Wells GN (2014) Unified form language: a domain-specific language for weak formulations of partial differential equations. ACM Trans Math Softw(TOMS) 40(2):1–37. https://doi.org/10.1145/2566630

Ambrosio L, Buttazzo G (1993) An optimal design problem with perimeter penalization. Calc Var Partial Differ Equ 1(1):55–69. https://doi.org/10.1007/BF02163264

Babadjian JF, Francfort G, Mora M (2012) Quasi-static evolution in nonassociative plasticity: The cap model. SIAM J Math Anal 44(1):245–292. https://doi.org/10.1137/110823511

Balay S, Gropp WD, McInnes LC, Smith BF (1997) Efficient management of parallelism in object oriented numerical software libraries. In: Arge E, Bruaset AM, Langtangen HP (eds) Modern software tools in scientific computing. Birkhäuser Press, Boston, pp 163–202

Balay S, Abhyankar S, Adams MF, Benson S, Brown J, Brune P, Buschelman K, Constantinescu E, Dalcin L, Dener A, Eijkhout V, Gropp WD, Hapla V, Isaac T, Jolivet P, Karpeev D, Kaushik D, Knepley MG, Kong F, Kruger S, May DA, McInnes LC, Mills RT, Mitchell L, Munson T, Roman JE, Rupp K, Sanan P, Sarich J, Smith BF, Zampini S, Zhang H, Zhang H, Zhang J (2021a) PETSc/TAO users manual. Tech. Rep. ANL-21/39—Revision 3.16, Argonne National Laboratory

Balay S, Abhyankar S, Adams MF, Benson S, Brown J, Brune P, Buschelman K, Constantinescu EM, Dalcin L, Dener A, Eijkhout V, Gropp WD, Hapla V, Isaac T, Jolivet P, Karpeev D, Kaushik D, Knepley MG, Kong F, Kruger S, May DA, McInnes LC, Mills RT, Mitchell L, Munson T, Roman JE, Rupp K, Sanan P, Sarich J, Smith BF, Zampini S, Zhang H, Zhang H, Zhang J (2021b) PETSc Web page. https://petsc.org/

Baumrucker B, Renfro J, Biegler L (2008) MPEC problem formulations and solution strategies with chemical engineering applications. Comput Chem Eng 32(12):2903–2913. https://doi.org/10.1016/j.compchemeng.2008.02.010

Bendsøe M, Sigmund O (2003) Topology optimization: theory, methods and applications, 2nd edn. Springer, New York

Bourdin B (2001) Filters in topology optimization. Int J Numer Meth Eng 50(9):2143–2158. https://doi.org/10.1002/nme.116

Bourdin B, Chambolle A (2003) Design-dependent loads in topology optimization. ESAIM: control. Optim Calcul Variat 9:19–48. https://doi.org/10.1051/cocv:2002070

Bourdin B, Chambolle A (2006) The phase-field method in optimal design. In: IUTAM Symposium on topological design optimization of structures, machines and materials. Springer, New York, pp 207–215. https://doi.org/10.1007/1-4020-4752-5

Bourdin B, Francfort GA, Marigo JJ (2008) The variational approach to fracture. J Elast 91(1–3):1–148. https://doi.org/10.1007/s10659-007-9107-3

Braides A (1998) Approximation of free-discontinuity problems. In: Lecture Notes in Mathematics, vol 1694. Springer, New York. https://doi.org/10.1007/BFb0097344

Chouly F (2013) On convergence of the penalty method for unilateral contact problems. Appl Numer Math 65:27–40. https://doi.org/10.1016/j.apnum.2012.10.003

Dal Maso G, DeSimone A, Mora MG (2006) Quasistatic evolution problems for linearly elastic–perfectly plastic materials. Arch Ration Mech Anal 180(2):237–291. https://doi.org/10.1007/s00205-005-0407-0

Desmorat B, Desmorat R (2008) Topology optimization in damage governed low cycle fatigue. Compte Rendus Mécanique 336(5):448–453. https://doi.org/10.1016/j.crme.2008.01.001

Drabla S, Sofonea M, Teniou B (1998) Analysis of a frictionless contact problem for elastic bodies. Ann Polon Math 69(1):75–88. https://doi.org/10.4064/ap-69-1-75-88

Duysinx P, Bendsøe M (1998) Topology optimization of continuum structures with local stress constraints. Int J Numer Meth Eng 43:1453–1478. https://doi.org/10.1016/j.cma.2016.02.024

Farrell PE, Ham DA, Funke SW, Rognes ME (2013) Automated derivation of the adjoint of high-level transient finite element programs. SIAM J Sci Comput 35(4):C369–C393. https://doi.org/10.1137/120873558

Francfort G, Marigo JJ (1993) Stable damage evolution in a brittle continuous medium. Eur J Mech A/Solids 12(2):149–189

Francfort GA, Marigo JJ (1998) Revisiting brittle fracture as an energy minimization problem. J Mech Phys Solids 46(8):1319–1342. https://doi.org/10.1016/S0022-5096(98)00034-9

Fukushima M, Pang JS (1999) Convergence of a smoothing continuation method for mathematical progams with complementarity constraints. In: Lecture notes in economics and mathematical systems. Springer, Berlin, pp 99–110. https://doi.org/10.1007/978-3-642-45780-7_7

Haber R, Jog C, Bendsøe M (1996) A new approach to variable-topology shape design using a constraint on the perimeter. Struct Optim 11:1–12. https://doi.org/10.1007/BF01279647

Haslinger J, Klarbring A (1993) Shape optimization in unilateral contact problems using generalized reciprocal energy as objective functional. Nonlinear Anal 21(11):815–834. https://doi.org/10.1016/0362-546x(93)90048-w

Hintermüller M, Kopacka I (2011) A smooth penalty approach and a nonlinear multigrid algorithm for elliptic MPECs. Comput Optim Appl 50(1):111–145. https://doi.org/10.1007/s10589-009-9307-9

Hsueh CJ, Bhattacharya K (2018) Optimizing microstructure for toughness: the model problem of peeling. Struct Multidiscip Optim 58(3):1067–1080. https://doi.org/10.1007/s00158-018-1952-0

Hu XM, Ralph D (2004) Convergence of a penalty method for mathematical programming with complementarity constraints. J Optim Theory Appl 123(2):365–390. https://doi.org/10.1007/s10957-004-5154-0

Kinderlehrer D, Stampacchia G (2000) An introduction to variational inequalities and their applications, classics in applied mathematics, vol 31. SIAM, Philadelphia, PA

Kirby RC (2004) FIAT, a new paradigm for computing finite element basis functions. ACM Trans Math Softw (TOMS) 30(4):502–516. https://doi.org/10.1145/1039813.1039820

Kirby RC (2012) FIAT: numerical construction of finite element basis functions. In: Automated solution of differential equations by the finite element method. Springer, New York, pp 247–255. https://doi.org/10.1007/978-3-642-23099-8

Kirby RC, Logg A (2006) A compiler for variational forms. ACM Trans Math Softw (TOMS) 32(3):417–444. https://doi.org/10.1145/1163641.1163644

Kočvara, Outrata JV (1995) On the solution of optimum design problems with variational inequalities. In: Recent advances in nonsmooth optimization. World Scientific, Singapore, pp 172–192. https://doi.org/10.1142/9789812812827_0011

Li P, Wu Y, Yvonnet J (2021) A SIMP-phase field topology optimization framework to maximize quasi-brittle fracture resistance of 2d and 3d composites. In: Theoretical and applied fracture mechanics, p 102919. https://doi.org/10.1016/j.tafmec.2021.102919

Lipton R, Stuebner M (2006) Optimization of composite structures subject to local stress constraints. Comput Methods Appl Mech Eng 196(1–3):66–75. https://doi.org/10.1016/j.cma.2006.01.012

Logg A, Wells GN (2010) DOLFIN: automated finite element computing. ACM Trans Math Softw 37(2):1–28. https://doi.org/10.1145/1731022.1731030

Logg A, Mardal KA, Wells GN (2012) Automated solution of differential equations by the finite element method: the FEniCS book, vol 84. Springer, New York

Logg A, Ølgaard KB, Rognes ME, Wells GN (2012b) Ffc: the fenics form compiler. In: Automated solution of differential equations by the finite element method. Springer, New York, pp 227–238. https://doi.org/10.1007/978-3-642-23099-8_11

Logg A, Wells GN, Hake J (2012c) DOLFIN: A C++/Python finite element library. In: Automated solution of differential equations

by the finite element method. Springer, New York, pp 173–225. https://doi.org/10.1007/978-3-642-23099-8

Luo ZQ, Pang JS, Ralph D (1996) Mathematical programs with equilibrium constraints. Cambridge University Press, Cambridge

Maury A (2016) Shape optimization for contact and plasticity problems thanks to the level set method. PhD thesis, Université Pierre et Marie Curie

Maury A, Allaire G, Jouve F (2017) Shape optimisation with the level set method for contact problems in linearised elasticity. SMAI J Comput Math 3:249–292. https://doi.org/10.5802/smai-jcm.27

Maury A, Allaire G, Jouve F (2018) Elasto-plastic shape optimization using the level set method. SIAM J Control Optim 56(1):556–581. https://doi.org/10.1137/17M1128940

Maute K, Schwarz S, Ramm E (1998) Adaptive topology optimization of elastoplastic structures. Struct Multidiscip Optim 15(2):81–91. https://doi.org/10.1007/BF01278493

Mignot F, Puel J (1984) Optimal control in some variational inequalities. SIAM J Control Optim 22(3):466–476. https://doi.org/10.1137/0322028

Mitusch S, Funke S, Dokken J (2019) dolfin-adjoint 2018.1: automated adjoints for FEniCS and firedrake. J Open Source Softw 4(38):1292

Moré JJ, Thuente DJ (1994) Line search algorithms with guaranteed sufficient decrease. ACM Trans Math Softw (TOMS) 20(3):286–307. https://doi.org/10.1145/192115.192132

Ølgaard KB, Wells GN (2010) Optimizations for quadrature representations of finite element tensors through automated code generation. ACM Trans Math Softw (TOMS) 37(1):1–23. https://doi.org/10.1145/1644001.1644009

Outrata J, Zowe J (1995) A numerical approach to optimization problems with variational inequality constraints. Math Program 68(1):105–130. https://doi.org/10.1007/BF01585759

Outrata JV (1994) On optimization problems with variational inequality constraints. SIAM J Optim 4(2):340–357. https://doi.org/10.1137/0804019

Scholtes S (2001) Convergence properties of a regularization scheme for mathematical programs with complementarity constraints. SIAM J Optim 11(4):918–936. https://doi.org/10.1137/S1052623499361233

Si H (2015) Tetgen, a delaunay-based quality tetrahedral mesh generator. ACM Trans Math Softw 41(2):11:1-11:36. https://doi.org/10.1145/2629697

Sokolowski J, Zolesio JP (1992) Introduction to shape optimization. Springer, Berlin, Heidelberg

Tran NV (2021) The active set method for optimal designs with obstacle constraints. https://doi.org/10.5281/zenodo.5716559